FULL LENGTH ARTICLE

Antagonizing exosomal miR-18a-5p derived from prostate cancer cells ameliorates metastasis-induced osteoblastic lesions by targeting Hist1h2bc and activating Wnt/β-catenin pathway

Fanchun Zeng [a,b], Chunrong Zhao [b], Rujie Wang [c], Lingyan Ren [d], Hao Qiu [c], Zhi Zou [a,b], Haibin Ding [b], Zhongyi Sun [e,***], Jianmei Li [b,**], Shiwu Dong [b,*]

[a] *Key Laboratory for Biorheological Science and Technology of Ministry of Education, State and Local Joint Engineering Laboratory for Vascular Implants, College of Bioengineering, Chongqing University, Chongqing 400030, China*
[b] *Department of Biomedical Materials Science, Army Medical University, Chongqing 400038, China*
[c] *Department of Orthopedics, Xinqiao Hospital, Army Medical University, Chongqing 400038, China*
[d] *Antenatal Diagnosis Centre, Guizhou Provincial People's Hospital, Guiyang, Guizhou 550003, China*
[e] *Department of Urology, Shenzhen University General Hospital, Shenzhen University, Shenzhen, Guangdong 518055, China*

Abstract More than 50% of prostate cancer (PCa) patients have bone metastasis with osteoblastic lesions. MiR-18a-5p is associated with the development and metastasis of PCa, but it remains unclear whether it is involved in osteoblastic lesions. We first found that miR-18a-5p was highly expressed in the bone microenvironment of patients with PCa bone metastases. To address how miR-18a-5p affects PCa osteoblastic lesions, antagonizing miR-18a-5p in PCa cells or pre-osteoblasts inhibited osteoblast differentiation *in vitro*. Moreover, injection of PCa cells with miR-18a-5p inhibition improved bone biomechanical properties and bone

  * Corresponding author. Department of Biomedical Materials Science, Army Medical University, 30 Gaotanyan, Shapingba District, Chongqing 400038, China.
 ** Corresponding author. Department of Biomedical Materials Science, Army Medical University, 30 Gaotanyan, Shapingba District, Chongqing 400038, China.
*** Corresponding author. Department of Urology, Shenzhen University General Hospital, Shenzhen University, Shenzhen, Guangdong 518055, China.
    E-mail addresses: sunzhy199481@hotmail.com (Z. Sun), lijianmei@tmmu.edu.cn (J. Li), dongshiwu@163.com (S. Dong).
    Peer review under responsibility of Chongqing Medical University.

mineral mass *in vivo*. Furthermore, miR-18a-5p was transferred to osteoblasts by exosomes derived from PCa cells and targeted the *Hist1h2bc* gene, resulting in Ctnnb1 up-regulation in the Wnt/β-catenin signaling pathway. Translationally, antagomir-18a-5p significantly improved bone biomechanical properties and alleviated sclerotic lesions from osteoblastic metastases in BALB/c nude mice. These data suggest that inhibition of exosome-delivered miR-18a-5p ameliorates PCa-induced osteoblastic lesions.

Introduction

Prostate cancer (PCa) is the most common cancer in men, accounting for more than 1 in 5 new diagnoses.[1] More than half of PCa patients would develop bone metastasis, especially in advanced stage.[2,3] Although the 5-year relative survival rate for PCa combined diagnosed during 2009 through 2015 was 98%, many patients are presented with metastatic cancer but they succumb to the disease despite treatment. PCa metastases are an important cause of death and could reduce patients' quality of life.[4] Patients with PCa usually develop bone metastases with osteoblastic lesions, which cause severe pain, pathological fractures, and spinal cord compression.[5]

The osteoblastic lesions of PCa bone metastasis are mainly pathological bone formation, which involves changes in bone biomechanical properties.[6] PCa cells secrete several osteoblast-stimulating factors to trigger bone formation, such as cellular communication network factor 3, transmembrane serine protease 2 to ETS-related gene, endothelin-1 (ET-1), vascular endothelial growth factor, bone morphogenetic protein 1 or 4, platelet derived growth factor, insulin like growth factor 1, transforming growth factor beta 1, plasminogen activator, kallikrein related peptidase 3 and sonic hedgehog signaling molecule.[7−14] PC-3 cells belong to human PCa cells that could cause osteolytic lesions,[15] but recent studies found that PC-3 cell-derived vesicles promote osteoblast differentiation.[12,16] In addition, PCa cells also indirectly induce osteoblastic lesions by inhibiting osteoclast differentiation or acting on endothelial cells.[17−19] Therefore, it is a common feature that PCa cells lead to osteoblastic lesions. Although previous studies reported multiple factors that contributed to osteoblastic lesions of PCa bone metastasis, its pathogenesis was complicated, and in-depth studies remains required to realize its clinical treatment.

MiR-18a-5p is a conserved and multifunctional miRNA in the miR-17-92 cluster and overexpressed in PCa.[20−22] Lu's team showed that the expression of miR-18a-5p in PCa tissue was significantly higher than that in normal prostate tissues,[20] and the expression of miR-18a-5p in patients with PCa metastasis was significantly higher than that in non-metastatic patients.[22,23] In addition, inhibiting miR-18a-5p could sensitize the effect of PCa radiotherapy.[24] Thus, miR-18a-5p might play an important role in the occurrence and metastasis of PCa. Moreover, periodontal ligament stem cells treated with bisphosphonate differentiate into osteoblasts and showed an increased expression of miR-18a-5p

in compared with the untreated group.[25] Therefore, miR-18a-5p may play an important role in osteoblastic lesions of PCa bone metastasis.

In our study, we observed elevated miR-18a-5p expression in human PCa bone metastases. Furthermore, we clarified the molecular mechanism of osteoblastic lesions caused by overexpression of miR-18a-5p in PCa cells, and finally found that antagomir-18a-5p could safely and effectively treat osteoblastic lesions in PCa bone metastases.

Materials and methods

Human bone metastasis specimens

This medical research was approved by the Ethics Committee of the Third Military Medical University (AF/SC-08/1.0). The Xinqiao Hospital of the Third Military Medical University stocks samples of bone metastasis lesions were previously harvested from PCa patients from 2011 to 2020, including 4 bone samples from PCa bone metastases and 3 samples of bone fractures (Table S1).

Cell culture

In this study, we used human PCa cell lines (PC-3 and C4-2B) and normal immortalized cells from prostate (WPMY-1 cells). PC-3, C4-2B, WPMY-1 and MC3T3-E1 clone 4 cell lines were obtained from American Type Culture Collection (ATCC, USA). PC-3, C4-2B, and WPMY-1 cells were cultured in H-DMEM medium (HyClone, USA) containing 10% FBS. The MC3T3-E1 clone 4 cell lines were maintained in α-MEM medium (HyClone, USA) containing 10% FBS. Primary bone marrow mesenchymal stem cells (BMSCs) from C57BL/6J mice were cultured in α-MEM medium (HyClone, USA) containing 10% FBS. The osteogenic induction medium contained 1% penicillin streptomycin, 10% FBS, 10 mmol/L β-sodium glycerophosphate, 0.1 μmol/L dexamethasone and 50 mg/L ascorbic acid. In the coculture experiment, osteoblasts were cultured with 40% tumor cell supernatant. All culture media were replaced with fresh medium every 3 days.

Animal models

Animal experiments were approved by the Laboratory Animal Welfare and Ethics Committee of the Third Military Medical University (AMUWEC20211686). Male BALB/C nude mice (6−8 weeks old) were obtained from SIPEIFU Biology

(Beijing, China) and reared adaptively in a constant humidity and temperature environment for 2−4 weeks for experiments. PCa cells (1×10^5) were suspended in ∼25 μL of phosphate buffer saline (PBS) and injected into the right tibia of nude mice with an insulin syringe. PBS was injected into the left tibia of nude mice as an internal control. *In vivo* imaging was performed for tumor detection at 4 weeks after treatment. The mice were sacrificed by overdose injection of chloral hydrate solution at 4 weeks or 5 weeks after treatment, and the tibias were obtained for biomechanical testing or fixed them in 4% paraformaldehyde. As for the therapeutic experiments, the antagomir-18a-5p was diluted to 1 mg/mL with PBS (Table S2). Each nude mouse was injected with 0.1 mg antagomir-18a-5p intraperitoneally, and the control group was injected with an equal volume of PBS once every two weeks, twice in total. Four weeks after treatment, the mice were sacrificed by overdose injection of chloral hydrate solution, and then obtained the liver, kidney and tibia for biomechanical testing or fixed them in 4% paraformaldehyde.

qPCR

Total RNA was extracted from cells using TRIzol. Then, the total RNA was reversely transcribed into cDNA with the reverse transcription Kit (Takara, Japan) strictly followed the instructions of the manufacturer. Subsequently, the SYBR Green qPCR Kit (Takara, Japan) was used for qPCR, and the mRNA expressions were calculated using Gapdh as internal reference. MiRNA was extracted with a miRNA Purification Kit (CWBIO, China) and then a miRNA cDNA Synthesis Kit (CWBIO, China) and miRNA qPCR Assay Kit (CWBIO, China) were used for qPCR-based measurement of the expression levels of miRNA. U6 or cel-miR-39 was used as control. Table S3 listed the qPCR primers used in this study.

Western blot

RIPA lysate containing 1% protease inhibition was used to lyse cells and extract protein. Protein concentration was detected by BCA Protein assay kit (Beyotime, China). Exosomes (EXO) (10 μg) or proteins (30 μg) extracted from cells were diluted 1:4 (v/v) in a loading buffer (Beyotime, China), heated at 95 °C for 10 min, loaded onto 10% gels (CWBIO, China), electrophoresed at 110 V for 60−70 min, and transferred to membranes by using the PVDF (Merck, USA) 120 min program. For all subsequent antibody-incubation and washing steps, a rocking platform was used. After blocking with blocking buffer for 2 h, the membranes were incubated with primary antibodies at 4 °C overnight, washed in TBST, incubated with secondary antibodies at room temperature for 90 min, washed with TBST, and then exposed to a detection reagent (Biosharp, China) for visualization. The primary antibodies were as follows: CD9 (BIOSS, China, 1:1000), CD63 (CST, USA, 1:1000), TFIIB (CST, USA, 1:1000), H3 (BIOSS, China, 1:1000), Runx2 (Affinity, USA, 1:1000), Col1 (Abcam, USA, 1:1000), Gapdh (BIOSS, China, 1:1000), Sp7 (Affinity, USA, 1:1000), Bglap (Affinity, USA, 1:1000), Hist1h2bc (ABCEPTA, China, 1:1000) and Ctnnb1 (Affinity, China, 1:1000).

Micro-CT analysis

Micro-CT analysis was performed with a resolution of 6.6 μm. The micro-CT files were reconstructed by NRecon software, and 3D images were generated by CTVox. The micro-CT analyzer software was used for data analysis, and the parameters of bone mineral density (BMD) and bone volume per tissue volume (BV/TV) were quantified. BMD changes and BV/TV changes referred to the changes in the right tibia compared with the corresponding left tibia (control) in the same nude mice. The specific calculation method was as follows (R for right tibia, L for left tibia):

$$BMD\ Change = 100*(BMD_R - BMD_L)/BMD_L$$

$$BV/TV\ Change = 100*(BV/TV_R - BV/TV_L)/BV/TV_L$$

Biomechanical test

The biomechanical test was performed by the vertical compression method, and the loading force (F) and the deformation distance ($\triangle$l) were recorded. The maximum displacement was set to 6 mm, and the loading speed was set at 0.01 mm/s. The diameter (d) and length (l_0) of the tibia were measured with a vernier caliper. The maximum stress was the ultimate load. The stress (σ) and elastic modulus (Y, Young's modulus) were calculated as follows (R for right tibia, L for left tibia):

$$\sigma = F/S = F/(\pi(d/2)^2)$$

$$Ultimate\ load\ change = 100*(\sigma_R - \sigma_L)/\sigma_L$$

$$Yang's\ modulus = Stress/strain = \sigma/(\triangle l/l_0)$$

$$Yang's\ modulus\ change = 100*(Y_R - Y_L)/Y_L$$

Histological analyses

The specimens were fixed in 4% paraformaldehyde, decalcified rapidly, and embedded in paraffin wax. Subsequently, specimens were sectioned at 5-μm thickness with a tissue slicer (Leica, Germany). Finally, HE (Solarbio, China), Sirius red (Solarbio, China), Masson (Solarbio, China), and TRAP staining (Wako, Japan), RNA *in situ* hybridization (BOSTER, China) and immunohistochemistry (Solarbio, China) were performed according to the manufacturer's instructions. In immunohistochemistry, the diluted concentration of prostate-specific antigen (PSA) antibody was 1:100 (BIOSS, China, 1:100).

Alkaline phosphatase (ALP) and Alizarin red S staining

For ALP staining, osteoblasts were stained with a BCIP/NBT Kit (CWBIO, China) after 7 or 14 days of osteogenic induction. For Alizarin red S staining, osteoblasts were stained

with an Alizarin red S Kit (Solarbio, China) after 7 or 14 days of osteogenic induction. ALP and Alizarin red S staining were performed according to the manufacturer's instructions.

Lentivirus transfection

Lentiviral plasmids encoding miR-18a-5p-mimic, miR-18a-5p-inhibition and a negative control were constructed by HANBIO (Shanghai, China) (Table S2). C4-2B, PC-3, MC3T3-E1 and BMSC cells were transfected with the lentivirus at a multiplicity of infection of 10, after which selection was performed in 7.5 μg/mL puromycin for 1 week. Lentiviral plasmids encoding Hist1h2bc-mimic, Hist1h2bc-siRNA and their negative control were constructed by HANBIO (Shanghai, China). MC3T3-E1 cells were transfected with the lentivirus at a multiplicity of infection of 10, after which selection was performed in 10 μg/mL blasticidin for 1 week.

Transcriptome sequencing

Collect MC3T3-E1 cells transfected with miR-18a-5p-mimic lentivirus and negative MC3T3-E1 cells. RNA extraction and transcriptome sequencing were conducted by a commercial service (BGI, China). The raw readings were collected with a DNBSEQ-T7 (BGI, China) platform. The DESeq2 package was used for differential gene analysis. We screened for differential gene analysis by using these criteria: |log2 (FC)| > 1 (FC: fold-change) and $P < 0.05$. Transcriptional sequencing data could be obtained in the Sequence Read Archive (SRA) database, accession to cite for these SRA data: PRJNA735584.

Exosome isolation and identification

EXO were isolated from cell culture supernatants with 10% exosome-depleted FBS (HyClone, USA) through differential centrifugation. After 48 h of culture, when cells were 90% confluent, the supernatant was harvested and centrifuged at $300 \times g$ for 10 min, $3000 \times g$ for 10 min, $10,000 \times g$ for 30 min, and then $40,000 \times g$ for 30 min. Next, the supernatant was centrifuged at $110,000 \times g$ for 2 h (Hitachi, Japan). The pellet was resuspended in PBS, and the sample was purified with a 0.2 μm filter. A BCA protein assay kit (Beyotime, China) was used for exosome quantification, and exosome morphology was analyzed by transmission electron microscopy (Tecnai, USA). To examine exosome size distribution, Dynamic Light Scattering (DLS) was performed with a ZetaPALS instrument (Brookhaven, USA).[26]

Statistical analyses

Statistics data were expressed as mean ± SD or SEM. Analyses were performed by GraphPad Prism version 8.0. Paired data were analyzed by paired t-test. Unpaired data were analyzed by unpaired t-test. $P < 0.05$ was indicated statistical significance.

Results

MiR-18a-5p was highly expressed in osteoblastic lesions of PCa bone metastasis

Previous study showed that the abundance of miR-18a-5p was higher in the prostate tissues and serum of metastatic PCa patients than that in non-metastatic patients,[20,22,23] but it was unknown in the bone microenvironment of PCa bone metastasis. Four bone specimens were collected from patients with PCa bone metastasis, and three cases of fracture were collected as the control group (Table S1). Immunohistochemical studies showed that prostate-specific antigen (PSA) was positive in clinical bone specimens (Fig. 1A). Pathological results showed that young bone was formed in the bone metastasis site of patients (Fig. 1B). However, in the same position in Figure 1B, osteoclast activity was not enhanced (Fig. 1C). We detected the abundance of miR-18a-5p in clinical bone specimens. In situ hybridization results showed that miR-18a-5p exhibited higher expression in the osteoblastic lesions microenvironment of PCa patients than that in control group (Fig. 1D).

We found that miR-18a-5p was significantly increased in two classical PCa bone metastasis cells compared with normal immortalized prostate cells (WPMY-1) (Fig. 1E). In the process of PCa bone metastasis, C4-2B cells showed osteoblastic phenotype in the early stage,[27] but showed osteoblastic and osteolytic phenotype in the late stage.[28] PC-3 cells are considered to induce osteolytic phenotype,[28] but it is unclear whether PC-3 cells cause osteoblastic phenotype in the early stage. Therefore, PCa cells were implanted into the right tibia of nude mice, and an equal volume of phosphate buffer saline (PBS) was implanted into the left tibia as an internal control group (Fig. 1F). The PCa bone metastatic model was confirmed by intravital imaging after implantation into the tibia for 4 weeks (Fig. 1G). Micro-CT analysis showed that PC-3 cells were associated with severe osteolytic lesions and decreased bone mineral density (BMD) of cortical bone, but PC-3 cells caused slight osteoblastic lesions and formed bone spur alike on the surface of bone (Fig. 1H). C4-2B cells caused an associated severe intramedullary osteoblastic phenotype and increased BMD of cortical bone (Fig. 1H). We detected the abundance of miR-18a-5p in bone microenvironment of nude mice model. In addition, both osteoblastic phenotype and osteolytic phenotype were demonstrated to reduce the mechanical properties of bone.[6] However, C4-2B increased bone mechanical properties in osteoblastic phenotype (Fig. 1I, J), which may lead to osteosclerosis. In situ hybridization results showed that miR-18a-5p exhibited high expression in the bone microenvironment of the nude mice model with PCa bone metastasis (Fig. 1K). These results suggested that miR-18a-5p might be involved in PCa bone metastatic osteoblastic lesions.

Antagonizing miR-18a-5p in PCa cells inhibited osteoblasts differentiation and osteoblastic lesions

To investigate the effect of miR-18a-5p expressed by PCa cells on osteoblasts, lentivirus containing miR-18a-5p inhibition was transfected into PCa cells (C4-2B and PC-3)
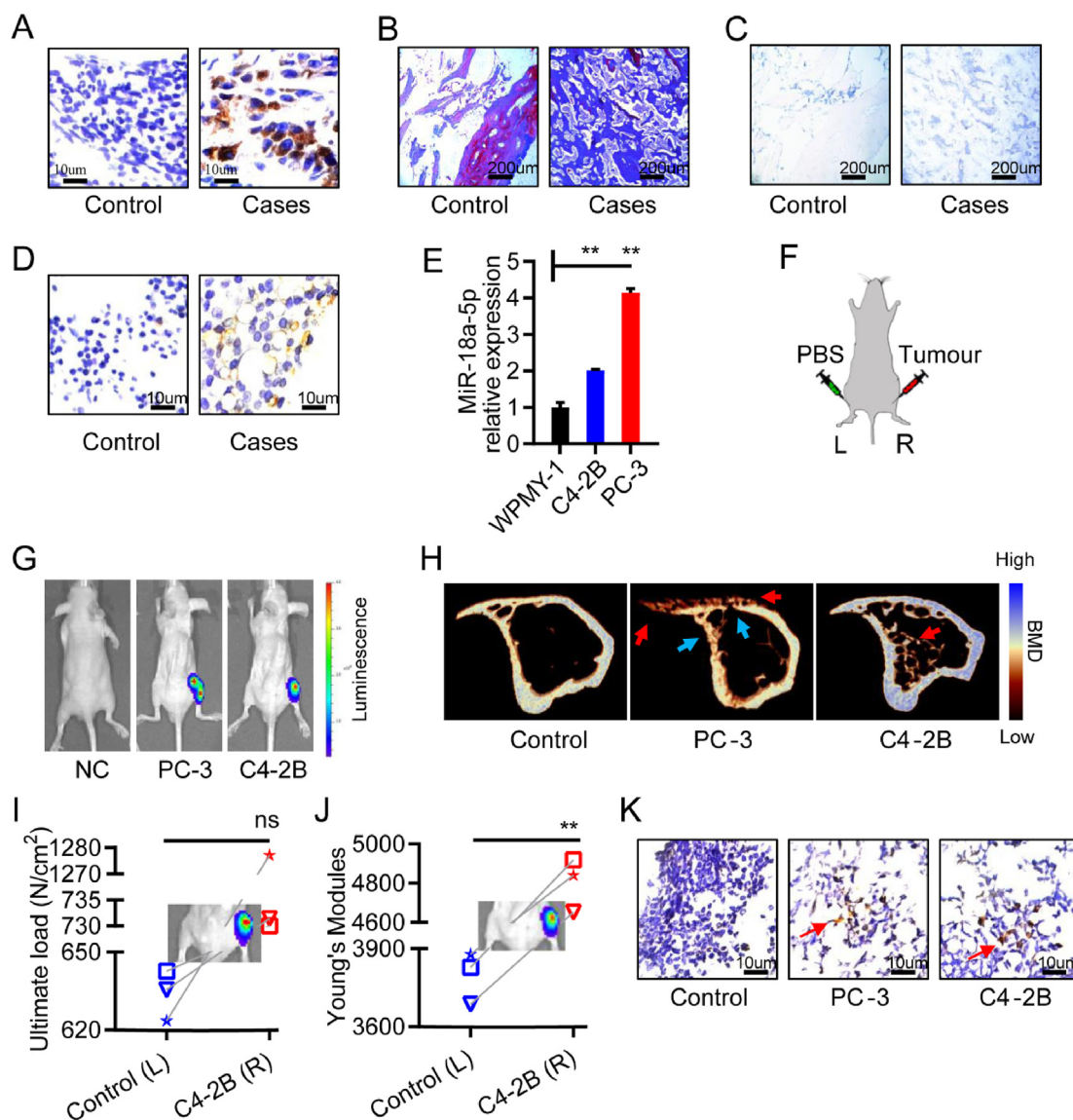
Figure 1 MiR-18a-5p was overexpressed in osteoblastic lesions of PCa bone metastasis. **(A–D)** Bone specimens of PCa patients with bone metastasis. (A) Immunohistochemical labeling of PSA (brown represents positive). (B) Masson staining (blue represents young bone, red represents old bone). (C) TRAP staining (purple represents positive). (D) *In situ* hybridization of miR-18a-5p (brown represents positive). **(E)** The miR-18a-5p expression in prostate cells and PCa bone metastasis cells. **(F)** Schematic diagram of the PCa bone metastasis model in nude mice (L represents left tibia; R represents right tibia). **(G)** *In vivo* imaging of nude mice implanted with PBS or PCa cells for 4 weeks. **(H–K)** Tibia specimens of PCa bone metastasis in nude mice after PCa cells implantation for 4 weeks. (H) Representative micro-CT 3D-reconstruction models illustrating in tibia (red arrows indicates an osteoblastic lesion; blue arrows indicate an osteolytic lesion). (I) The ultimate load of tibia implanted with C4-2B cells. (J) The Young's modules of tibia implanted with C4-2B cells. (K) *In situ* hybridization of miR-18a-5p (brown represents positive). The data are represented as mean ± SEM or SD. *$P < 0.05$, **$P < 0.01$, ***$P < 0.001$, ns $P > 0.05$.

(Fig. S1A, B) and set as the inhibition group, while empty vector-transfected PCa cells were established as the control group. C4-2B cell supernatant without intervention was set as cell supernatant (CS) group, and equal volume PBS was set as normal control (NC) group. Osteogenic-induced MC3T3-E1 cells were cocultured with the collected supernatant. After 7-d osteogenic induction, C4-2B cell supernatant promoted the expression of osteogenic marker protein, while miR-18a-5p-inhibited C4-2B cell supernatant inhibited the expression of osteogenic marker protein

(Fig. 2A). The ALP staining results showed that the miR-18a-5p-inhibited PCa cell supernatant inhibited osteoblasts activity (Fig. 2B). Finally, the results of Alizarin red S staining showed that mineralization was inhibited by the miR-18a-5p-inhibited PCa cells supernatant (Fig. 2C). These studies indicated that antagonizing miR-18a-5p in PCa cells could significantly inhibit osteoblast differentiation.

In the inhibition group ($n = 10$), C4-2B cells transfected with miR-18a-5p inhibition were implanted into the right tibias of the nude mice; in the control group ($n = 9$),

normal C4-2B cells were implanted into the right tibias of the nude mice, while the corresponding left tibias of all nude mice were implanted with an equal volume of PBS as an internal control group (Fig. 1F). Tibia specimens were collected after implanting for 4 weeks. C4-2B cells highly expressed PSA.[29] Immunohistochemical results showed that PSA was positive in PCa cells resident in the bone microenvironment (Fig. 2D), which indicated that C4-2B cells were successfully implanted there. Micro-CT analysis showed that bone hyperplasia was significant in the control group, while osteoblastic lesions were decreased in the inhibition group (Fig. 2E). Further study showed that the BMD change in inhibition group was significantly lower than that in control group (Fig. 2F). The results showed that the bone volume per tissue volume (BV/TV) change was significantly lower in inhibition group than that in control group (Fig. 2G). Then, HE, Sirius red and Masson staining showed that the osteoblastic lesions were significantly lower in inhibition group than in control group (Fig. 2H). Moreover, TRAP staining showed that miR-18a-5p-inhibited C4-2B cells did not affect osteoclastic activity (Fig. 2I). Similar to C4-2B cells, miR-18a-5p-inhibited PC-3 cells decreased osteoblastic lesions (Fig. 2J). However, PC-3 cells still had high osteolytic ability (Fig. 2K). In short, these results suggested that antagonizing miR-18a-5p in PCa cells could inhibit osteoblastic lesions.

Antagonizing miR-18a-5p in pre-osteoblasts inhibited osteoblast differentiation

Next, we explored whether pre-osteoblasts transfected with miR-18a-5p inhibition can inhibit osteoblast differentiation. During the osteogenic differentiation of normal MC3T3-E1 cells, the expression of miR-18a-5p was up-regulated (Fig. 3A). Then, lentivirus containing miR-18a-5p inhibition was transfected into MC3T3-E1 cells (Fig. S1C) and set as the inhibition group, while empty vector-transfected MC3T3-E1 cells were established as the control group. After 7 or 14 d of osteogenic induction, the mRNA expression of osteogenic differentiation marker genes was lower than that in control group (Fig. 3B, C). Similar results were observed in primary mouse bone marrow mesenchymal stem cells (BMSCs) transfected with lentivirus as MC3T3-E1 cells (Fig. S1D). After 14 or 21 d of osteogenic induction of BMSCs, the expression of the osteogenic differentiation marker proteins was lower than that in control group (Fig. 3D). After 14 or 21 d of osteogenic induction of MC3T3-E1 or BMSCs, the ALP staining showed that osteoblast activity was inhibited in both the inhibition groups (Fig. 3E). After 21 d of osteogenic induction, Alizarin red S staining also showed that reduced mineralization in both the inhibition groups (Fig. 3F). In conclusion, antagonizing miR-18a-5p in pre-osteoblasts could inhibit osteoblast differentiation and activity.

MiR-18a-5p targeted the *Hist1h2bc* gene to up-regulate Ctnnb1 expression

In fact, the exact molecular mechanism underlying miR-18a-5p promotes osteogenic differentiation remains unclear. Lentivirus containing miR-18a-5p mimic was transfected into MC3T3-E1 (Fig. S1C) and set as the mimic group, lentivirus containing miR-18a-5p inhibition was transfected into MC3T3-E1 and set as the inhibition group, while empty vector-transfected MC3T3-E1 were established as the control group. We performed transcriptome sequencing analysis on MC3T3-E1 transfected with lentivirus containing miR-18a-5p mimic, and found that 88 genes were up-regulated and 77 genes were down-regulated (Fig. 4A), and the accuracy of sequencing data was verified by qPCR (Fig. S2A). The bioinformatics analysis of the miR-18a-5p target gene revealed none common gene between the down-regulated genes and the miR-18a-5p target genes in the TargetScan database (7.2 version) (Fig. S2B).[30] The possible miR-18a-5p target genes from 77 down-regulated genes were manually screened by Clustal Omega,[31] and the results showed that miR-18a-5p might target the 3′UTR of the *Hist1h2bc* (*H2bc4*) gene (Fig. 4B). Then, results from the dual-luciferase reporter assay suggested that miR-18a-5p targeted *Hist1h2bc* (Fig. 4C). After 7 d of osteogenic induction of MC3T3-E1, the *Hist1h2bc* gene mRNA expressions were lower in mimic group than those in control group, but were up-regulated in inhibition group compared with control group (Fig. 4D). Finally, during the osteogenic differentiation of MC3T3-E1 cells, the expression of Hist1h2bc was down-regulated (Fig. 4E), and the expression trend was approximately opposite with miR-18a-5p (Fig. 3A). These results suggested that miR-18a-5p targeted *Hist1h2bc* gene during osteoblast differentiation.

Wnt/β-catenin signaling pathway plays an important role in osteoblast differentiation and PCa bone metastasis.[32−35] Therefore, we explored whether miR-18a-5p activates Wnt/β-catenin signaling pathway. Firstly, qPCR results showed that the mRNA expression of the key gene β-catenin (*Ctnnb1*) and the downstream gene myelocytomatosis oncogene (*Myc*) was higher in mimic group than that in control group but was down-regulated in inhibition group compared with control group (Fig. 4G). Similarly, nucleus proteins and cytoplasmic proteins were detected respectively, Western blot results showed that the expression of the key protein Ctnnb1 and the downstream protein Myc was higher in mimic group than that in control group but was down-regulated in inhibition group compared with control group (Fig. 4F). These results suggested that miR-18a-5p activated Wnt/β-catenin signaling pathway. Furthermore, we found that the expression of hist1h2bc was approximately opposite to that of Ctnnb1 (Fig. 4F). Subsequently, MC3T3-E1 were co-transfected with mimic or inhibition/siRNA of miR-18a-5p and hist1h2bc. After 7 d of osteogenic induction, qPCR results showed that the up-regulation of Ctnnb1 expression by miR-18a-5p was rescued by the hist1h2bc-iRNA (Fig. 4H). All of these results suggest that miR-18a-5p up-regulate the expression of Ctnnb1 by targeting *hist1h2bc*, thereby activating the Wnt/β-catenin signaling pathway.

MiR-18a-5p overexpressed by PCa was transferred to pre-osteoblasts via exosomes

Exosomes (EXO) were an efficient vector for intercellular material transportation. Next, we investigated whether miR-18a-5p secreted by PCa cells was transferred to pre-
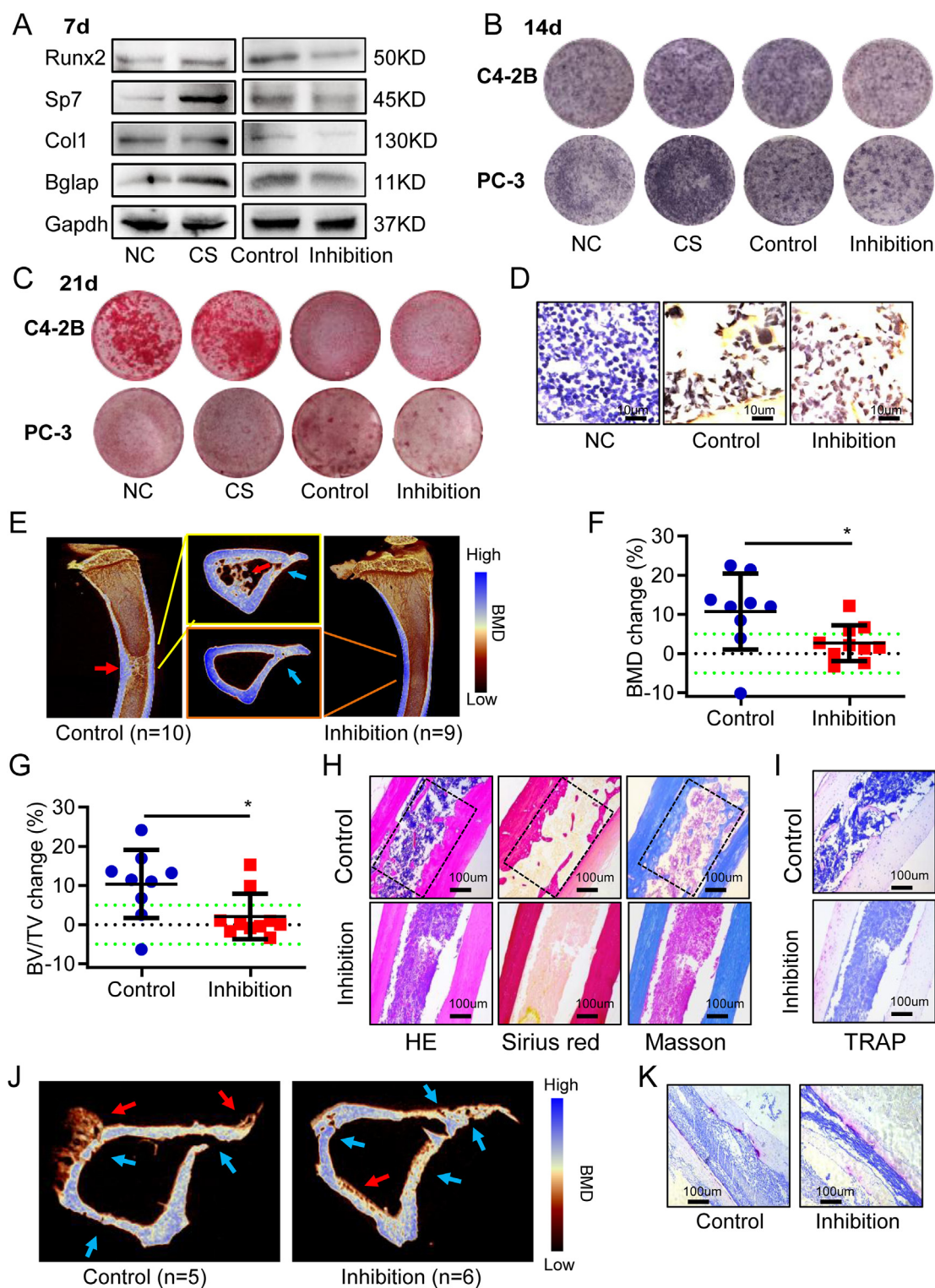
Figure 2 Antagonizing miR-18a-5p in PCa cells inhibited osteogenic differentiation and osteoblastic lesions. CS, PCa cells without intervention; Control, PCa cells with empty virus; Inhibition, PCa cells with miR-18a-5p inhibition; NC, Equal volume PBS. Osteogenic-induced MC3T3-E1 cells cocultured with PCa cells supernatant. **(A)** Osteogenic-induced 7 d, the expression of osteogenic differentiation marker proteins. PCa cells were C4-2B. **(B)** Osteogenic-induced 14 d, ALP staining. (PCa cells were C4-2B or PC-3). **(C)** Osteogenic-induced 21 d, Alizarin red S staining. (PCa cells were C4-2B or PC-3). **(D—I)** After 4 weeks of C4-2B implantation, the tibia specimens of PCa bone metastasis nude mice model. (D) PSA Immunohistochemistry (brown represents positive). (E) Representative 3D-reconstruction images of tibia. (F) BMD analysis. (G) BV/TV analysis. (H) HE, Sirius red (red represents bone) and Masson staining (blue represents bone). (I) TRAP staining (purple represents positive). **(J, K)** After 4 weeks of PC-3 implantation, the tibia specimens of PCa bone metastasis nude mice model. (J) Representative 3D-reconstruction images of tibia. (K) TRAP
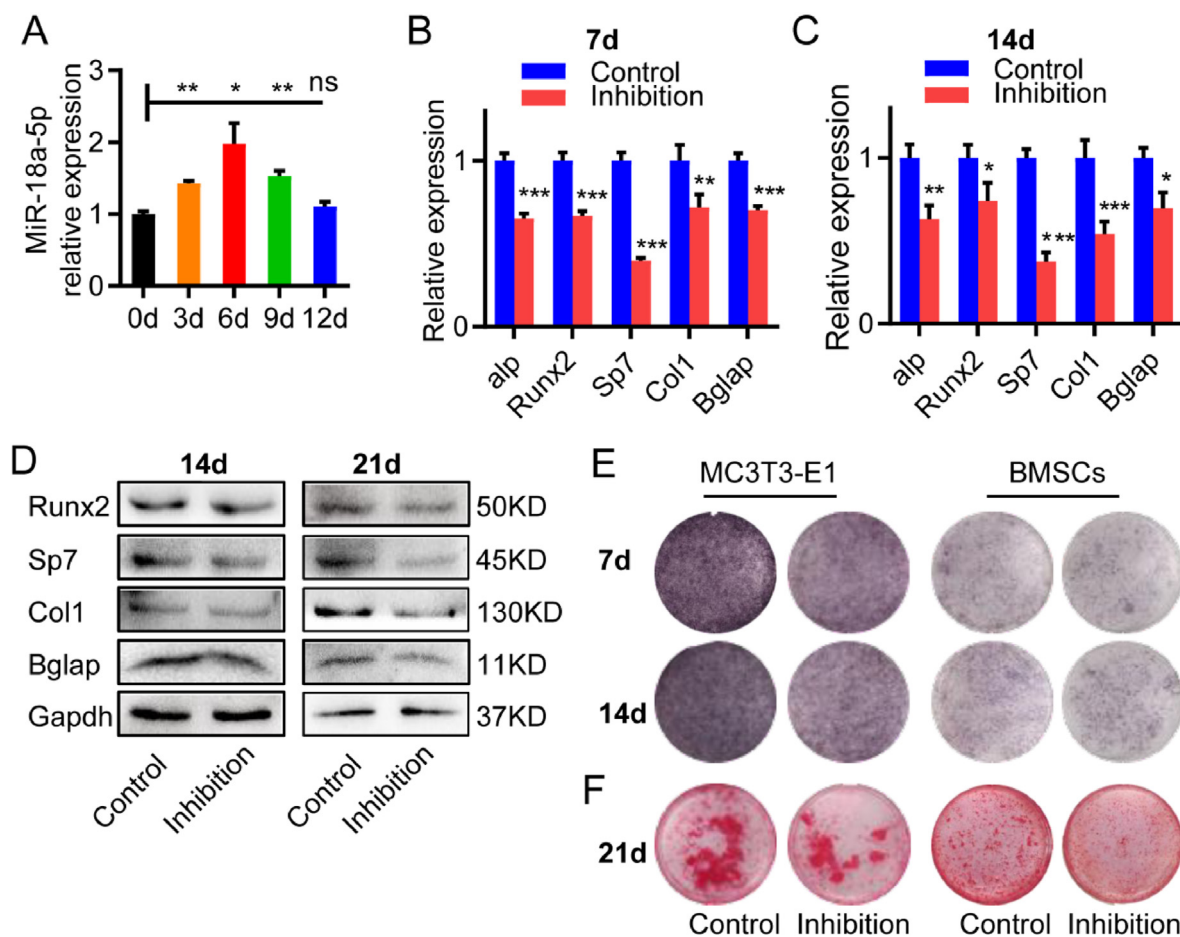
Figure 3 Antagonizing miR-18a-5p in pre-osteoblasts inhibited osteoblasts differentiation. Control, pre-osteoblasts with empty virus; Inhibition, pre-osteoblasts with miR-18a-5p inhibition. Pre-osteoblasts were MC3T3-E1 or BMSCs. **(A)** The expression of miR-18a-5p during osteogenic differentiation of MC3T3-E. **(B, C)** After 7 or 14 d of osteogenic induction of MC3T3-E1, the mRNA expression of osteogenic differentiation marker genes. **(D)** After 14 or 21 d of osteogenic induction of BMSCs, the expression of osteogenic differentiation marker protein. **(E)** After 7 or 14 d of osteogenic induction of MC3T3-E1 or BMSCs, ALP staining. **(F)** After 21 d of osteogenic induction of MC3T3-E1 or BMSCs, Alizarin red S staining. The data are represented as mean $\pm$ SEM or SD. *$P < 0.05$, **$P < 0.01$, ***$P < 0.001$, ns $P > 0.05$.

osteoblasts via EXO. EXO were isolated from WPMY-1, C4-2B, and PC-3 cells by ultracentrifugation. The morphology of EXO was identified with transmission electron microscopy (Fig. 5A). Moreover, the examination of the size distribution of EXO by using Dynamic Light Scattering (DLS) revealed that the majority of the population was in the ~150 nm range (Fig. 5B). Western blot analysis showed that the exosome markers (CD63 and CD9) were both positive in exosomes derived from WPMY-1 cells (WPMY-1-EXO), exosomes derived from C4-2B cells (C4-2B-EXO), and exosomes derived from PC-3 cells (PC-3-EXO), but the nucleoprotein TFIIB was negative (Fig. 5C). MC3T3-E1 cells were treated with C4-2B-EXO. After 7 or 14 d of osteogenic induction, the expressions of marker proteins of osteogenic differentiation were higher in C4-2B-EXO group than those in NC group (Fig. 5D), and the ALP staining showed its activity was

higher in C4-2B-EXO group than that in NC group (Fig. 5E). After 21 d of osteogenic induction, Alizarin red S staining also showed promoted calcification in C4-2B-EXO group (Fig. 5F). Moreover, it has been proved that PC-3 cell-derived vesicles promote osteoblast differentiation.[12,16] These results indicated that C4-2B-EXO promoted osteoblast differentiation.

Next, qPCR was used to detect the abundance of miR-18a-5p in different periods of the transfer from C4-2B cells to MC3T3-E1. Compared with the normal prostate WPMY-1 cells, miR-18a-5p showed high abundance in C4-2B cells, cell supernatants and EXO (Fig. 5G). The miR-18a-5p abundance in MC3T3-E1 cells increased significantly after cocultured with C4-2B cell supernatant (Fig. 5G). GW4869 was a potent neutral sphingomyelinases inhibition, which prevented the formation of intraluminal vesicles to further block EXO production and
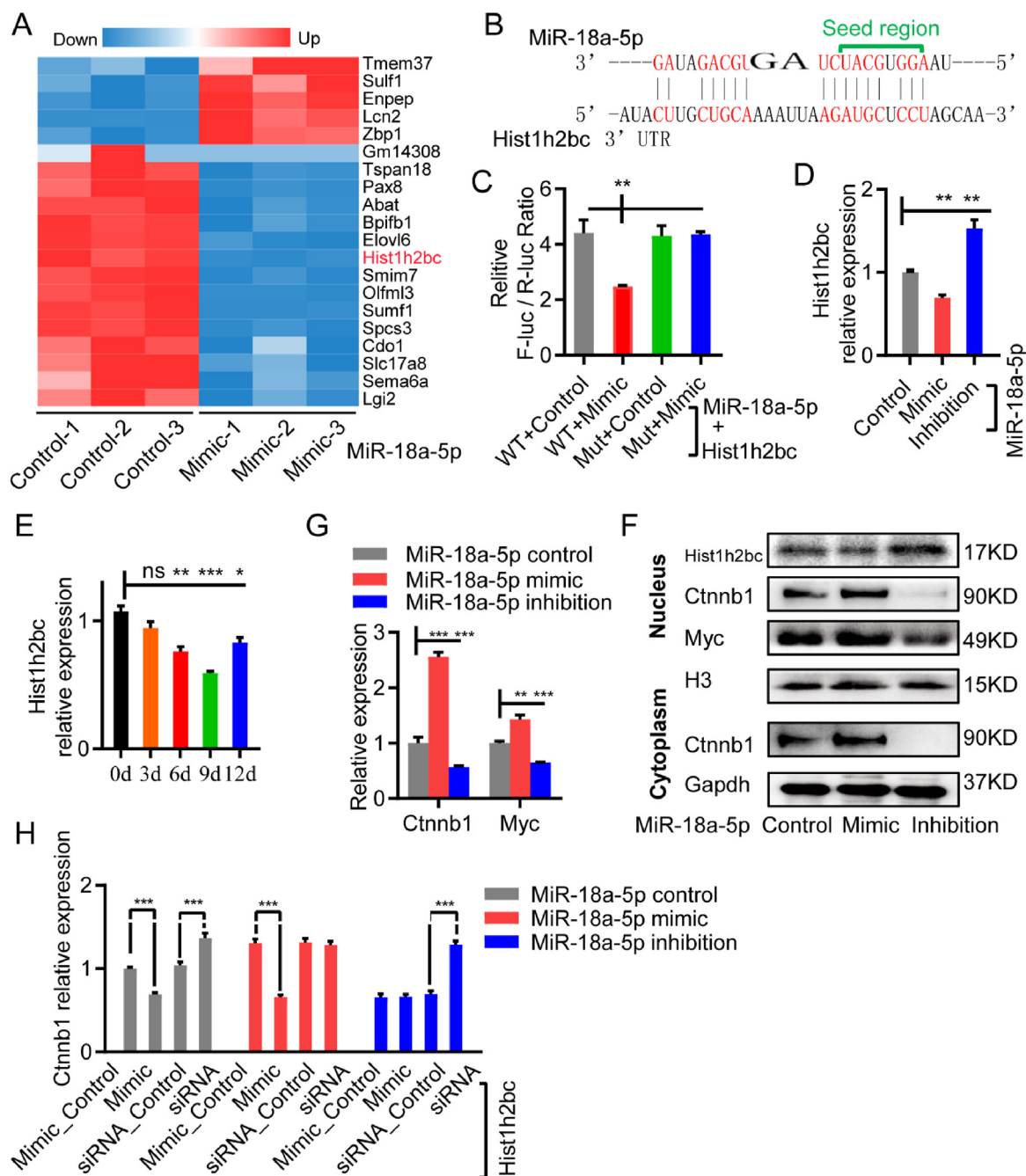
staining (purple represents positive). The data are represented as mean $\pm$ SEM or SD. *$P < 0.05$, **$P < 0.01$, ***$P < 0.001$, ns $P > 0.05$. The dotted green line indicates a range of 5%, which was considered to be normal.

Figure 4 MiR-18a-5p targeted the *Hist1h2bc* gene to promote osteoblast differentiation. (A) Differential genes heat map for transcriptome sequencing between mimic group and control group. (B) Schematic diagram of miR-18a-5p targeting the *Hist1h2bc* gene. (C) Dual-luciferase reporter assay of miR-18a-5p targeting the *Hist1h2bc* gene (WT represents wild-type *Hist1h2bc*, Mut represents the *Hist1h2bc* mutant, mimic represents miR-18a-5p mimics, and NC represents the miR-18a-5p negative control). (D) MC3T3-E1 transfected with miR-18a-5p mimic or inhibition were osteogenic-induced for 7 d, the mRNA expression of *Hist1h2bc* gene. (E) *Hist1h2hc* gene expression during osteoblast differentiation. (F, G) MC3T3-E1 transfected with miR-18a-5p mimic or inhibition were osteogenic-induced for 7 d. (F) mRNA qPCR. (G) Nucleus proteins and cytoplasmic proteins Western blot. (I) After 7 d osteogenic induction of MC3T3-E1 cells with miR-18a-5p or Hist1h2hc, mRNA qPCR. The data are represented as mean ± SEM or SD. *$P < 0.05$, **$P < 0.01$, ***$P < 0.001$, ns $P > 0.05$.

release in numerous cell types.[36] MC3T3-E1 cells were treated with PCa cell supernatant (CS), PCa cell supernatant with GW4869 (CS-GW4869), PCa-EXO (C4-2B-EXO or PC-3-EXO) respectively, and set equal volume of PBS as a control. After 3 h of treatment, *in situ* hybridization results showed low miR-18a-5p abundance in MC3T3-E1 treated with PBS or CS-GW4869, while high abundance of miR-18a-5p was found in MC3T3-E1 cells treated with CS or PCa-EXO (Fig. 5H). In conclusion, miR-18a-5p overexpressed by PCa was transferred to MC3T3-E1 cells via EXO.
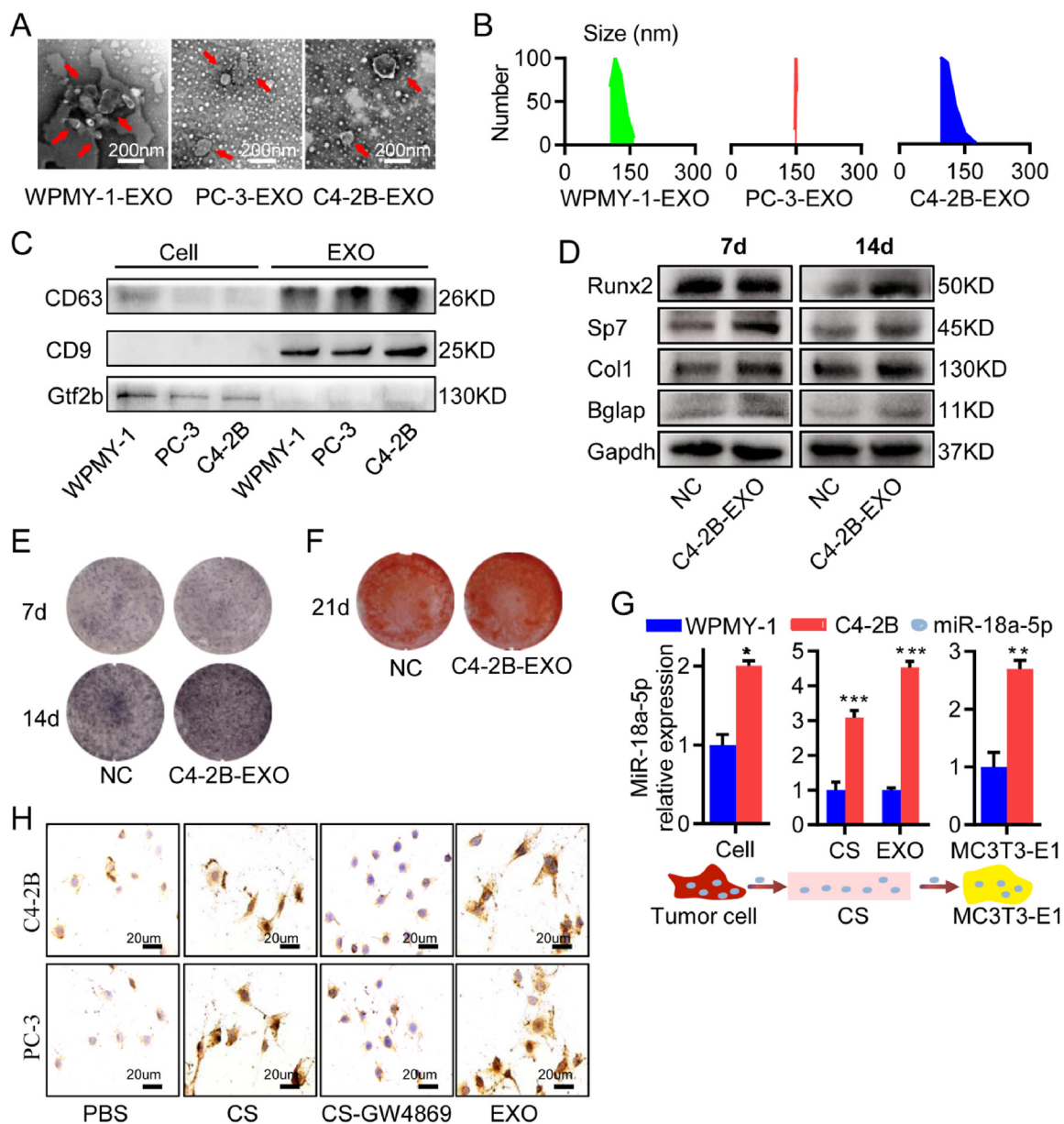
Figure 5 Exosome-transported miR-18a-5p was expressed by PCa cells. **(A)** Representative transmission electron microscopy images of PCa-EXO. **(B)** Average size distribution of PCa-EXO by using DLS. **(C)** Western blot detection of exosome marker proteins. **(D–F)** Osteogenic-induced MC3T3-E1 treated with C4-2B-EXO. **(D)** The expression of osteogenic differentiation marker proteins. **(E)** ALP staining. **(F)** Alizarin red S staining. **(G)** The mRNA abundance of miR-18a-5p in C4-2B cells, C4-2B cells supernatants (CS), C4-2B-EXO, and MC3T3-E1 cells cocultured with C4-2B cell supernatant, respectively. **(H)** *In situ* hybridization of miR-18a-5p in MC3T3-E1 cells by treated with CS, CS-GW4869 or EXO from PCa cells. Set PBS as control group, (brown represents positive). The data are represented as mean ± SEM or SD. *$P < 0.05$, **$P < 0.01$, ***$P < 0.001$, ns $P > 0.05$.

Antagomir-18a-5p alleviated osteoblastic lesions in PCa bone metastasis

We studied the treatment of osteoblastic lesions in PCa bone metastasis with antagomir-18a-5p. Firstly, we evaluated the safety of the antagomir-18a-5p in BALB/c nude mice. In the antagomir group ($n = 3$), healthy male nude mice were intraperitoneally injected with antagomir-18a-5p once every 2 weeks. The control group ($n = 3$) was treated with equal volume of PBS. All nude mice were sacrificed 4 weeks later. In the antagomir

group and the control group, no abnormality was observed in the liver, kidney or tibia by HE staining analysis (Fig. 6A; Fig. S3A), and no difference in osteoclast activity was observed in TRAP staining (Fig. S3B). These results suggested that the antagomir-18a-5p was safe in nude mice.

The model of PCa bone metastasis was established by implanting C4-2B cells into the right tibia of nude mice, and an equal volume of PBS was implanted into the left tibia. After C4-2B cells implantation for 1 week, the antagomir group ($n = 9$) was intraperitoneally injected with the
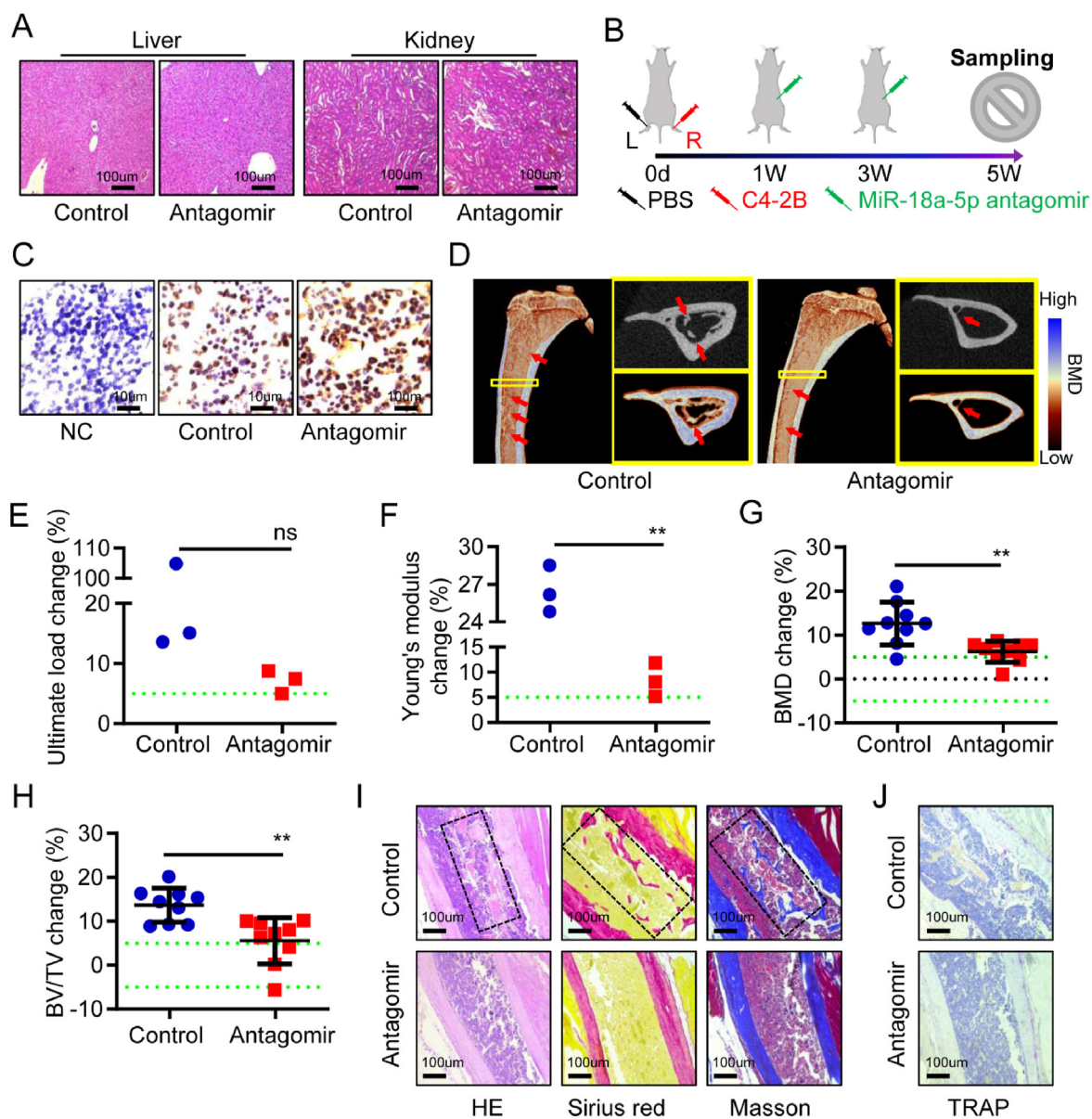
Figure 6 Antagomir-18a-5p treated osteoblastic lesions caused by PCa bone metastasis. **(A)** Safety evaluation of the liver and kidney in normal nude mice treated with antagomir-18a-5p or PBS for 4 weeks, HE staining. **(B)** Schematic diagram of the antagomir-18a-5p in the treatment of PCa bone metastases in nude mice. **(C–J)** Tibia specimens of PCa bone metastasis nude mice model after treatment for 4 weeks (control represents PBS treatment, antagomir represents antagomir-18a-5p treatment). **(C)** PSA immunohistochemistry (NC represents normal tibia microenvironment; brown represents positive). **(D)** Representative 3D-reconstruction images of tibia (red arrow indicates osteoblastic lesions). **(E)** The ultimate load changes. **(F)** Young's modulus change. **(G)** The BMD changes. **(H)** The BV/TV change. **(I)** HE, Sirius red (red represents bone) and Masson staining (blue represents bone). **(J)** TRAP staining (purple represents positive). The data are represented as mean ± SEM or SD. *$P < 0.05$, **$P < 0.01$, ***$P < 0.001$, ns $P > 0.05$. The dotted green line indicates a range of 5%, which was considered to be normal.

antagomir-18a-5p, and the control group ($n = 9$) was treated with PBS once every 2 weeks. Tibia specimens were collected after treatment for 4 weeks (Fig. 6B). The immunohistochemical results showed that PSA was positive in the tibia microenvironment of nude mice with PCa bone metastasis in the antagomir group and the control group (Fig. 6C). *In situ* hybridization showed miR-18a-5p expression of the tibia microenvironment was lower in antagomir group than that in control group (Fig. S4). Subsequently, micro-CT analysis showed that the osteoblastic lesions

caused by C4-2B cells was particularly severe after PBS treatment, while the lesions presented a mildly osteoblastic phenotype after antagomir-18a-5p treatment (Fig. 6D). Biomechanical analysis of vertical compression showed that the ultimate load change and Young's modulus change in the control group was greater than that in antagomir group (Fig. 6E, F). Further results showed that the BMD change and BV/TV change in the control group were significantly greater than those in the antagomir group (Fig. 6G, H). Finally, the pathological analysis of the

tibia was performed. HE, Sirius red and Masson staining indicated that there were more serious osteoblastic lesions in the control group, while the antagomir group had the slight osteoblastic lesions (Fig. 6I). The TRAP staining showed no significant difference in osteoclast activity between the antagomir group and the control group (Fig. 6J). In a word, these results indicated that the antagomir-18a-5p could effectively treat osteoblastic lesions caused by PCa bone metastasis.

Discussion

The progress against cancer reflected large declines in mortality for PCa. As of 2017, the death rate has dropped from its peak for PCa by 52% (since 1993).[1] However, the number of patients with bone metastases from PCa have been not decreased. The bone metastasis was observed in up to 70% of patients with PCa and mainly manifested as osteoblastic lesions, which were very painful for patients. Unclear pathogenesis was the main difficulty in treating PCa bone metastasis. Recent studies demonstrated that miR-18a-5p promotes the proliferation of PCa cells, whereas inhibition of miR-18a-5p expression attenuated the growth.[23,37,38] Furthermore, our study found that miR-18a-5p was overexpressed in the bone metastasis microenvironment of PCa patients. In addition, this study also found that the expression of miR-18a-5p was increased during osteoblasts differentiation. Moreover, *in vitro* antagonizing miR-18a-5p in PCa cells, MC3T3-E1 cells, and BMSCs proved that inhibited osteoblastic differentiation,

and *in vivo* experiments showed that antagomir-18a-5p ameliorated PCa-induced osteoblastic lesions (Fig. 7). These results indicated that miR-18a-5p played an important role in the development of osteoblastic lesions in PCa bone metastasis and miR-18a-5p might be a potential target for the treatment of osteoblastic lesions in PCa cells.

Wnt/β-catenin signaling plays a key role in bone tissue by determining the differentiation of stem cells into mature osteoblasts. It up-regulates the expression of osteoblast markers (such as Runx2, Sp7 and Bglap) and enhanced ossification.[39] In contrast, antagonist of Wnt/β-catenin signaling pathway inhibited the formation and differentiation of osteoblasts to induce the osteolytic phenotype.[34,40] PCa cells secrete ET-1 whose concentration is elevated in the plasma of patients with advanced PCa.[9] Clines et al confirmed that ET-1 stimulated the Wnt/β-catenin signaling pathway by inhibiting DKK1 to promote osteoblast differentiation for the formation of new bone.[10] Therefore, it is believed that the Wnt/β-catenin signaling pathway may play an important role in PCa metastasis-induced osteoblastic lesions. Of course, Mitani et al reported that the activation of Wnt/β-catenin signaling pathway promoted the proliferation of PCa cells.[4] Additionally, our study confirmed that miR-18a-5p expressed by PCa cells was transferred via EXO to pre-osteoblasts, and then miR-18a-5p up-regulated the *Ctnnb1* gene in osteoblasts by targeting the *Hist1h2bc* gene. *Ctnnb1*, a key gene of Wnt/β-catenin signaling pathway, promoted osteoblastic differentiation. Chen et al reported β-catenin protein promotes bone formation.[41] This result is consistent with our study. The
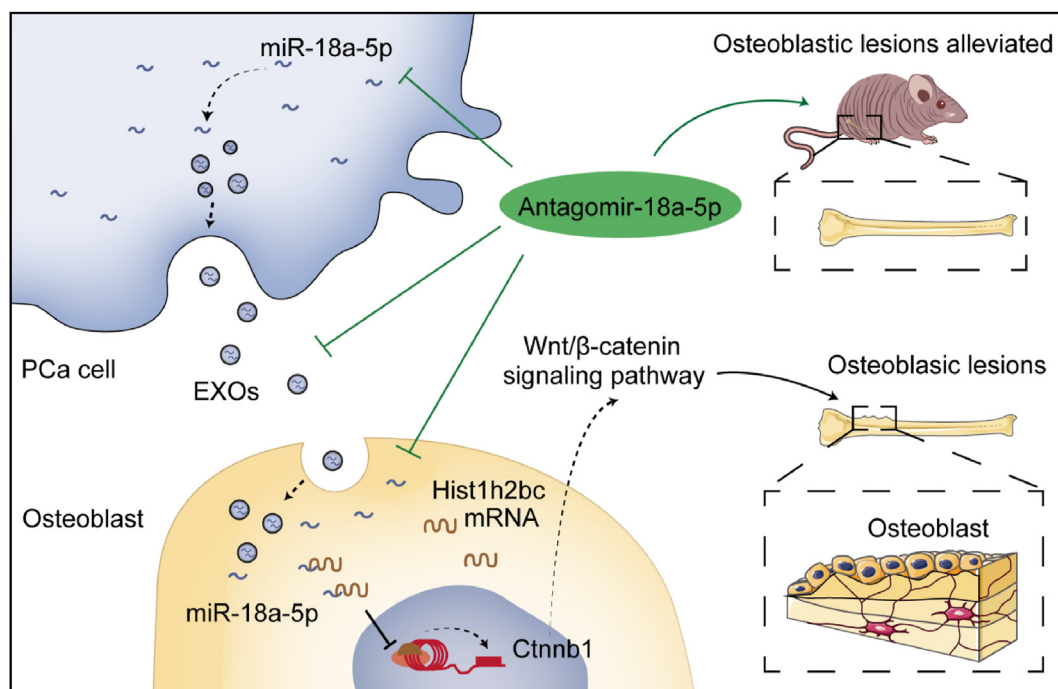

Figure 7 The molecular mechanism and therapeutic strategy of miR-18a-5p mediating osteoblastic lesions in PCa bone metastasis. PCa-EXO transports miR-18a-5p into osteoblasts, where miR-18a-5p targets the *Hist1h2bc* gene and promotes *Ctnnb1* gene expression, thereby positively regulating the Wnt/β-catenin signaling pathway and leading to osteoblastic lesions. Antagomir-18a-5p could effectively alleviated osteoblastic lesions.

Hist1h2bc gene encoded a replication-dependent histone which was a member of the histone H2B family and involved in the assembly of chromosomal nucleosome and cell differentiation.[42,43] However, there were few studies about the *Hist1h2bc* gene.[44] These studies revealed the molecular mechanism of PCa cells mediating miR-18a-5p to induce osteoblastic lesions.

EXO have been studied as an important transport vector in PCa bone metastasis.[45–48] However, there were still different views on the function of PCa-EXO on osteoblasts.[12,16,47,49] PCa cell-derived exosomes stimulate miR-141-3p to suppress *DLC1* gene expression in osteoblasts, thereby activating the p38-MAPK pathway and promoting osteoblast differentiation.[50] Sato et al revealed that miR-940 secreted by PCa cells through exosomes promoted osteogenic differentiation of MSCs by targeting ARHGAP1 and FAM134A.[27] Our findings miR-18a-5p overexpressed by PCa was transferred to pre-osteoblasts via EXO. It means that the goods of PCa-EXO play an important role in osteoblastic lesions.

PCa cells such as C4-2B cells induced hard osteoblastic lesions, which might lead to spinal cord compression and even hematopoietic dysfunction. Although another PCa cells PC-3 were mainly osteolytic lesions, the abnormal formation of bone spur alike induced by PC-3 cells might be one of the important causes of bone pain. At present, drugs for cancer bone metastasis in clinical applications or under development mainly focus on the treatment of osteolytic lesions,[51–54] while there are few drugs for the treatment of osteoblastic lesions. This study finally explored the treatment of osteoblastic lesions in PCa bone metastasis. Antagomir have been used in the treatment of tumor bone metastases or bone lesions *in vivo*.[55–57] In this study, we confirmed that the antagomir-18a-5p was safe *in vivo*. Subsequently, antagomir-18a-5p was used to treat nude mice with PCa bone metastases, and the results showed that the biomechanical properties, BMD and BV/TV were all significantly improved, and osteoblastic lesions were alleviated, which suggested that the antagomir-18a-5p had excellent therapeutic effect on PCa bone metastasis. It was speculated that antagomir-18a-5p had a prospect in preventing osteoblastic lesions in patients with PCa or early PCa bone metastasis. It would avoid bone sclerosis, spinal cord compression and alleviate bone pain. Although clinical trials of miRNA drugs encountered difficulties,[58] engineering exosomes for targeted drug delivery would help to improve the safety and target ability of miRNA drugs.[59] In brief, the study provided important data supporting for the application of antagomir-18a-5p in the treatment of PCa bone metastasis.

In conclusion, this study elucidated the molecular mechanism and explored therapeutic strategies for osteoblastic lesions in PCa bone metastasis. It was showed that miR-18a-5p overexpressed by PCa bone metastatic cells was released into the bone microenvironment via EXO and incorporated into osteoblasts. MiR-18a-5p targeted the *Hist1h2bc* gene, thereby up-regulated the expression of Ctnnb1 in the Wnt/β-catenin signaling pathway, resulting in promoting the differentiation of pre-osteoblasts towards osteoblasts. It was found that antagomir-18a-5p was safe and effective for the treatment of osteoblastic lesions in PCa bone metastasis *in vivo*.

Author contributions

Shiwu Dong, Jianmei Li and Zhongyi Sun mainly contributed to the design of the study and the writing, review, and revision of manuscript; Fanchun Zeng performed cell experiments, animal experiments, data analysis and manuscript writing; Chunrong Zhao and Haibing Ding participated in the data analysis; Lingyan Ren participated in the immunohistochemistry; Rujie Wang and Hao Qiu participated in the collection and analysis of clinical specimens; Zhi Zou participated in micro-CT analysis. All authors read and approved the final manuscript.

Conflict of interests

The authors declare that they have no conflict of interests.

Appendix A. Supplementary data

Supplementary data to this article can be found online at https://doi.org/10.1016/j.gendis.2022.06.007.

References

1. Siegel RL, Miller KD, Jemal A. Cancer statistics, 2020. *CA Cancer J Clin*. 2020;70(1):7–30.
2. Deek MP, Taparra K, Dao D, et al. Patterns of recurrence and modes of progression after metastasis-directed therapy in oligometastatic castration-sensitive prostate cancer. *Int J Radiat Oncol Biol Phys*. 2021;109(2):387–395.
3. Furesi G, Rauner M, Hofbauer LC. Emerging players in prostate cancer-bone niche communication. *Trends Cancer*. 2021;7(2):112–121.
4. DiNatale A, Fatatis A. The bone microenvironment in prostate cancer metastasis. *Adv Exp Med Biol*. 2019;1210:171–184.
5. Walz S, Maas M, Stenzl A, Todenhöfer T. Bone health issues in patients with prostate cancer: an evidence-based review. *World J Mens Health*. 2020;38(2):151–163.
6. Sekita A, Matsugaki A, Nakano T. Disruption of collagen/apatite alignment impairs bone mechanical function in osteoblastic metastasis induced by prostate cancer. *Bone*. 2017;97:83–93.
7. Chen PC, Liu SC, Lin TH, et al. Prostate cancer-secreted CCN3 uses the GSK3β and β-catenin pathways to enhance osteogenic factor levels in osteoblasts. *Environ Toxicol*. 2021;36(3):425–432.
8. Delliaux C, Tian TV, Bouchet M, et al. TMPRSS2:ERG gene fusion expression regulates bone markers and enhances the osteoblastic phenotype of prostate cancer bone metastases. *Cancer Lett*. 2018;438:32–43.

9. Nelson JB, Hedican SP, George DJ, et al. Identification of endothelin-1 in the pathophysiology of metastatic adenocarcinoma of the prostate. *Nat Med*. 1995;1(9):944—949.

10. Clines GA, Mohammad KS, Bao Y, et al. Dickkopf homolog 1 mediates endothelin-1-stimulated new bone formation. *Mol Endocrinol*. 2007;21(2):486—498.

11. Mohamedali KA, Li ZG, Starbuck MW, et al. Inhibition of prostate cancer osteoblastic progression with VEGF121/rGel, a single agent targeting osteoblasts, osteoclasts, and tumor neovasculature. *Clin Cancer Res*. 2011;17(8):2328—2338.

12. Probert C, Dottorini T, Speakman A, et al. Communication of prostate cancer cells with bone cells via extracellular vesicle RNA; a potential mechanism of metastasis. *Oncogene*. 2019; 38(10):1751—1763.

13. Zhang X. Interactions between cancer cells and bone microenvironment promote bone metastasis in prostate cancer. *Cancer Commun*. 2019;39(1):76.

14. Nishimori H, Ehata S, Suzuki HI, Katsuno Y, Miyazono K. Prostate cancer cells and bone stromal cells mutually interact with each other through bone morphogenetic protein-mediated signals. *J Biol Chem*. 2012;287(24):20037—20046.

15. Tsingotjidou AS, Zotalis G, Jackson KR, et al. Development of an animal model for prostate cancer cell metastasis to adult human bone. *Anticancer Res*. 2001;21(2A):971—978.

16. Itoh T, Ito Y, Ohtsuki Y, et al. Microvesicles released from hormone-refractory prostate cancer cells facilitate mouse preosteoblast differentiation. *J Mol Histol*. 2012;43(5):509—515.

17. Karlsson T, Lundholm M, Widmark A, Persson E. Tumor cell-derived exosomes from the prostate cancer cell line TRAMP-C1 impair osteoclast formation and differentiation. *PLoS One*. 2016;11(11):e0166284.

18. Lin SC, Lee YC, Yu G, et al. Endothelial-to-osteoblast conversion generates osteoblastic metastasis of prostate cancer. *Dev Cell*. 2017;41(5):467—480.

19. Ganguly SS, Hostetter G, Tang L, et al. Notch3 promotes prostate cancer-induced bone lesion development via MMP-3. *Oncogene*. 2020;39(1):204—218.

20. Hsu TI, Hsu CH, Lee KH, et al. MicroRNA-18a is elevated in prostate cancer and promotes tumorigenesis through suppressing STK4 in vitro and in vivo. *Oncogenesis*. 2014;3(4):e99.

21. Deng JH, Deng Q, Kuo CH, Delaney SW, Ying SY. MiRNA targets of prostate cancer. *Methods Mol Biol*. 2013;936:357—369.

22. Ibrahim NH, Abdellateif MS, Kassem SH, Abd El Salam MA, El Gammal MM. Diagnostic significance of miR-21, miR-141, miR-18a and miR-221 as novel biomarkers in prostate cancer among Egyptian patients. *Andrologia*. 2019;51(10):e13384.

23. Zhang G, Han G, Zhang X, et al. Long non-coding RNA FENDRR reduces prostate cancer malignancy by competitively binding miR-18a-5p with RUNX1. *Biomarkers*. 2018;23(5):435—445.

24. Yang J, Hao T, Sun J, Wei P, Zhang H. Long noncoding RNA GAS5 modulates α-Solanine-induced radiosensitivity by negatively regulating miR-18a in human prostate cancer cells. *Biomed Pharmacother*. 2019;112:108656.

25. Zhou Q, Zhao ZN, Cheng JT, et al. Ibandronate promotes osteogenic differentiation of periodontal ligament stem cells by regulating the expression of microRNAs. *Biochem Biophys Res Commun*. 2011;404(1):127—132.

26. Sun W, Zhao C, Li Y, et al. Osteoclast-derived microRNA-containing exosomes selectively inhibit osteoblast activity. *Cell Discov*. 2016;2:16015.

27. Hashimoto K, Ochi H, Sunamura S, et al. Cancer-secreted hsa-miR-940 induces an osteoblastic phenotype in the bone metastatic microenvironment via targeting ARHGAP1 and FAM134A. *Proc Natl Acad Sci USA*. 2018;115(9):2204—2209.

28. Jin R, Sterling JA, Edwards JR, et al. Activation of NF-kappa B signaling promotes growth of prostate cancer cells in bone. *PLoS One*. 2013;8(4):e60983.

29. Chung LW, Kao C, Sikes RA, Zhau HE. Human prostate cancer progression models and therapeutic intervention. *Hinyokika Kiyo*. 1997;43(11):815—820.

30. Agarwal V, Bell GW, Nam JW, Bartel DP. Predicting effective microRNA target sites in mammalian mRNAs. *Elife*. 2015;4: e05005.

31. Madeira F, Park YM, Lee J, et al. The EMBL-EBI search and sequence analysis tools APIs in 2019. *Nucleic Acids Res*. 2019; 47(W1):W636—W641.

32. Duan P, Bonewald LF. The role of the Wnt/β-catenin signaling pathway in formation and maintenance of bone and teeth. *Int J Biochem Cell Biol*. 2016;77(Pt A):23—29.

33. Maeda K, Kobayashi Y, Koide M, et al. The regulation of bone metabolism and disorders by Wnt signaling. *Int J Mol Sci*. 2019; 20(22):5525.

34. Kaplan Z, Zielske SP, Ibrahim KG, Cackowski FC. Wnt and β-catenin signaling in the bone metastasis of prostate cancer. *Life*. 2021;11(10):1099.

35. Mitani T, Harada N, Nakano Y, Inui H, Yamaji R. Coordinated action of hypoxia-inducible factor-1α and β-catenin in androgen receptor signaling. *J Biol Chem*. 2012;287(40): 33594—33606.

36. Trajkovic K, Hsu C, Chiantia S, et al. Ceramide triggers budding of exosome vesicles into multivesicular endosomes. *Science*. 2008;319(5867):1244—1247.

37. Liang B, Zhou C, Cui S, et al. Upregulation of miR-18a-5p promotes the proliferation of prostate cancer via inhibiting the expression of SLC40A1. *Pathol Res Pract*. 2021;224:153448.

38. Lu TT, Tao X, Li HL, Gai L, Huang H, Li F. LncRNA GAS5 enhances tumor stem cell-like medicated sensitivity of paclitaxel and inhibits epithelial-to-mesenchymal transition by targeting the miR-18a-5p/STK4 pathway in prostate cancer. *Asian J Androl*. 2022. https://doi.org/10.4103/aja2021117.

39. Day TF, Guo X, Garrett-Beal L, Yang Y. Wnt/beta-catenin signaling in mesenchymal progenitors controls osteoblast and chondrocyte differentiation during vertebrate skeletogenesis. *Dev Cell*. 2005;8(5):739—750.

40. Kasoha M, Bohle RM, Seibold A, Gerlinger C, Juhasz-Böss I, Solomayer EF. Dickkopf-1 (Dkk1) protein expression in breast cancer with special reference to bone metastases. *Clin Exp Metastasis*. 2018;35(8):763—775.

41. Chen J, Long F. β-catenin promotes bone formation and suppresses bone resorption in postnatal growing mice. *J Bone Miner Res*. 2013;28(5):1160—1169.

42. Bult CJ, Blake JA, Smith CL, Kadin JA, Richardson JE. Mouse genome database group. Mouse genome database (MGD) 2019. *Nucleic Acids Res*. 2019;47(D1):D801—D806.

43. Lyons SM, Cunningham CH, Welch JD, et al. A subset of replication-dependent histone mRNAs are expressed as polyadenylated RNAs in terminally differentiated tissues. *Nucleic Acids Res*. 2016;44(19):9190—9205.

44. Sun Q, Zhang K, Chen J, Xu Y, Liu Y, Zheng R. Traditional Chinese medicine classification of knee osteoarthritis with proteomics analysis. *Ann Palliat Med*. 2020;9(6):3750—3756.

45. Patil KC, Soekmadji C. Extracellular vesicle-mediated bone remodeling and bone metastasis: implications in prostate cancer. *Subcell Biochem*. 2021;97:297—361.

46. Borel M, Lollo G, Magne D, Buchet R, Brizuela L, Mebarek S. Prostate cancer-derived exosomes promote osteoblast differentiation and activity through phospholipase D2. *Biochim Biophys Acta, Mol Basis Dis*. 2020;1866(12):165919.

47. Yu L, Sui B, Fan W, et al. Exosomes derived from osteogenic tumor activate osteoclast differentiation and concurrently inhibit osteogenesis by transferring COL1A1-targeting miRNA-92a-1-5p. *J Extracell Vesicles*. 2021;10(3):e12056.

48. Akoto T, Saini S. Role of exosomes in prostate cancer metastasis. *Int J Mol Sci*. 2021;22(7):3528.

49. Ma Q, Liang M, Wu Y, et al. Small extracellular vesicles deliver osteolytic effectors and mediate cancer-induced osteolysis in bone metastatic niche. *J Extracell Vesicles*. 2021;10(4):e12068.

50. Ye Y, Li SL, Ma YY, et al. Exosomal miR-141-3p regulates osteoblast activity to promote the osteoblastic metastasis of prostate cancer. *Oncotarget*. 2017;8(55):94834—94849.

51. Fornetti J, Welm AL, Stewart SA. Understanding the bone in cancer metastasis. *J Bone Miner Res*. 2018;33(12):2099—2113.

52. Costa L, Major PP. Effect of bisphosphonates on pain and quality of life in patients with bone metastases. *Nat Clin Pract Oncol*. 2009;6(3):163—174.

53. Mollica V, Rizzo A, Rosellini M, et al. Bone targeting agents in patients with metastatic prostate cancer: state of the art. *Cancers*. 2021;13(3):546.

54. Suzman DL, Boikos SA, Carducci MA. Bone-targeting agents in prostate cancer. *Cancer Metastasis Rev*. 2014;33(2—3): 619—628.

55. Wang X, Guo B, Li Q, et al. miR-214 targets ATF4 to inhibit bone formation. *Nat Med*. 2013;19(1):93—100.

56. Li H, Xie H, Liu W, et al. A novel microRNA targeting HDAC5 regulates osteoblast differentiation in mice and contributes to primary osteoporosis in humans. *J Clin Invest*. 2009;119(12): 3666—3677.

57. Tang Y, Pan J, Huang S, et al. Downregulation of miR-133a-3p promotes prostate cancer bone metastasis via activating PI3K/AKT signaling. *J Exp Clin Cancer Res*. 2018;37(1):160.

58. Zhang S, Cheng Z, Wang Y, Han T. The risks of miRNA therapeutics: in a drug target perspective. *Drug Des Devel Ther*. 2021;15:721—733.

59. Liang Y, Duan L, Lu J, Xia J. Engineering exosomes for targeted drug delivery. *Theranostics*. 2021;11(7):3183—3195.